NORSAR Scientific Report No. 2-2008

Semiannual Technical Summary

1 January - 30 June 2008

Frode Ringdal (ed.)

Kjeller, August 2008

6.3 Initial studies of signals recorded by ARCES infrasound sensors

Sponsored by US Army Space and Missile Defence Command, Contract No. W9113M-05-C-0224

6.3.1 Introduction

An important aspect of the infrasonic studies is the availability of data from a distributed network of arrays. The Swedish infrasound array network provides a useful supplement to the seismic and infrasonic arrays in Norway and NW Russia. The Apatity infrasound array is a three-element array co-located with the nine-element Apatity short-period regional seismic array, which was installed in 1992 on the Kola Peninsula, Russia by the Kola Regional Seismological Centre (KRSC). For further details see Baryshnikov (2004). The 25 element ARCES array is a short-period regional seismic array, located in northern Norway. ARCES has no infrasound sensors, but because of special near surface installation conditions, many of its seismic sensors are also sensitive to infrasound signals (see e.g., Ringdal & Schweitzer, 2005). The Swedish Infrasound Network (Liszka, 2007) has been in operation since the beginning of the 1970s. Operated by the Swedish Institute of Space Physics, the network has until recently comprised four infrasound stations: Kiruna, Jämtön, Lycksele and Uppsala. The station in Uppsala was moved to Sodankylä, Finland, during the summer of 2006. The currently available network of arrays for infrasound processing in the Nordic region is shown in Figure 6.3.1.

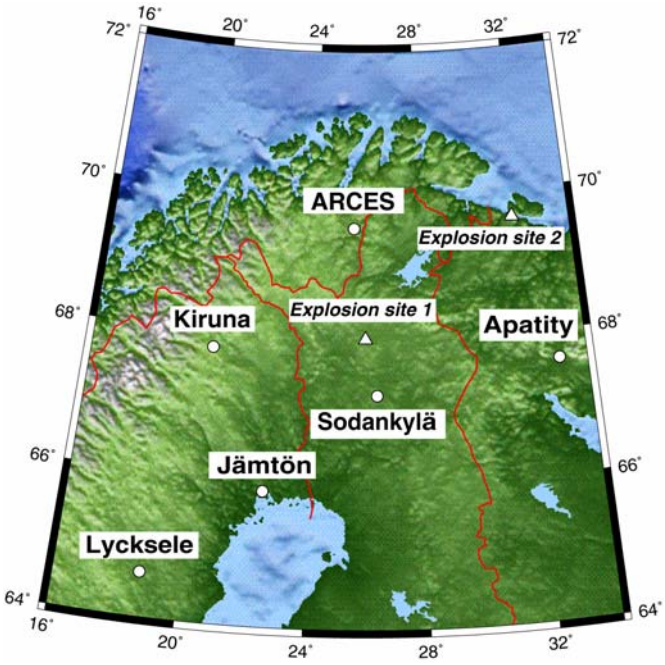

Figure 6.3.1. Locations of the arrays used for infrasonic processing in the Nordic countries. The site of the explosions in northern Finland discussed in previous papers (Explosion site 1) and the location of the presumed explosion in NW Russia discussed in detail in this paper (Explosion site 2) are marked on the map.

6.3.2 Experimental deployment of microbarographs within ARCES

The NORSAR staff has expended much effort during the past several years to determine a site for the projected IMS infrasound station near the ARCES array. Although these efforts until now have not been successful, we have made some progress in evaluating the infrasonic recording possibilities using dedicated infrasound sensors (as compared to using the seismic sensors of the ARCES array for infrasound recording). A recent development has been the installation of additional infrasonic recording equipment at three element near the center of ARCES, as illustrated in Figure 6.3.2. The data are digitized at a 40 Hz rate and extracted in parallel with the regular seismic data. The data from the infrasound sensors have been available at the NORSAR data center since about 1 April 2008.

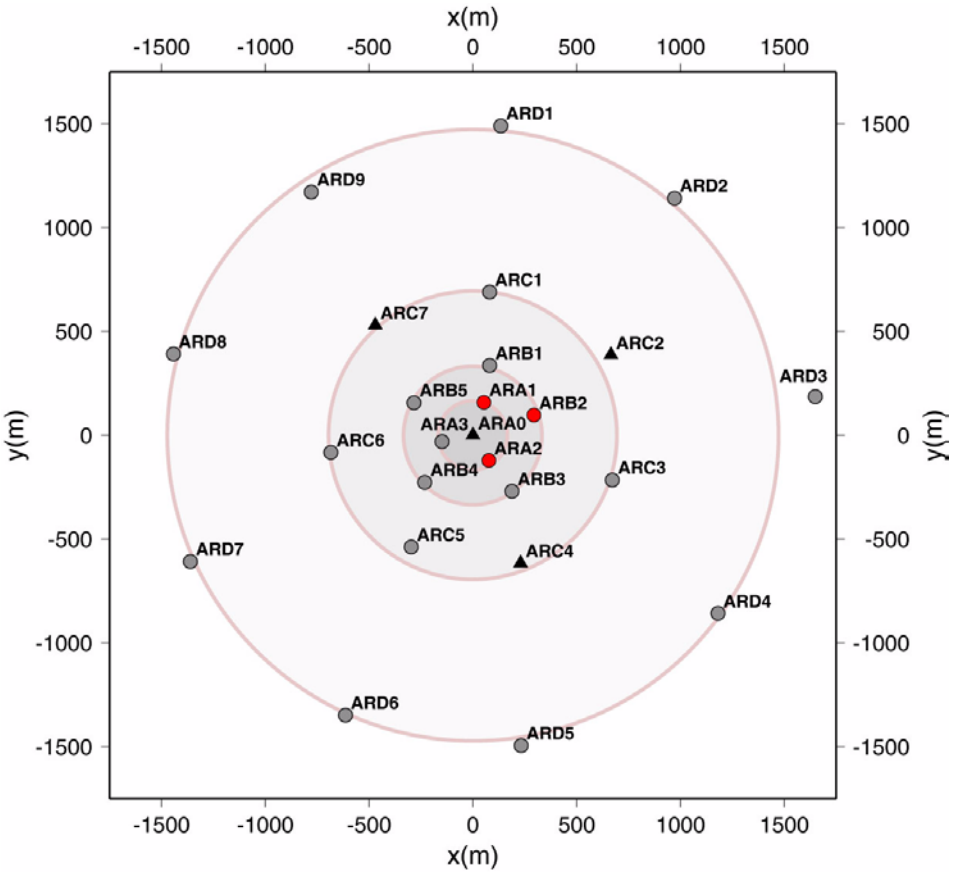

Figure 6.3.2. Configuration of the ARCES array. The filled circles denote vertical-component seismometers, and the triangles denote three-component seismometers. The three filled red circles represent the sites where infrasound sensors have been experimentally installed in addition to the seismic sensors. Also note that an experimental high-frequency seismic element has recently been installed at the center (ARA0) of the array.

6.3.3 Seismometers versus microbarographs for infrasound recording

We have begun an investigation aimed at comparing the quality of recording of infrasound signals when using seismometers versus recordings using microbarographs. Even taking into account the very efficient recording of such signals by the ARCES seismometers, our expectation would be that significant improvement would be obtained when using microbarographs. Nevertheless, the much larger number of seismic sensors would be a factor that should also be taken into account.

Figure 6.3.3 shows two waveforms covering 20 minutes of ARCES array data and representing the presumed explosion in NW Russia mentioned above. The top waveform shows seismometer data (ARA2) and the bottom waveform shows microbarograph data from the same site. We note that the seismometer data shows P and S phases from the presumed explosion as well as P and S phases from an unrelated seismic event (a mining event near Kiruna, Sweden). The infrasonic signal is very clear on both the traces and looks quite similar on the two sensors.

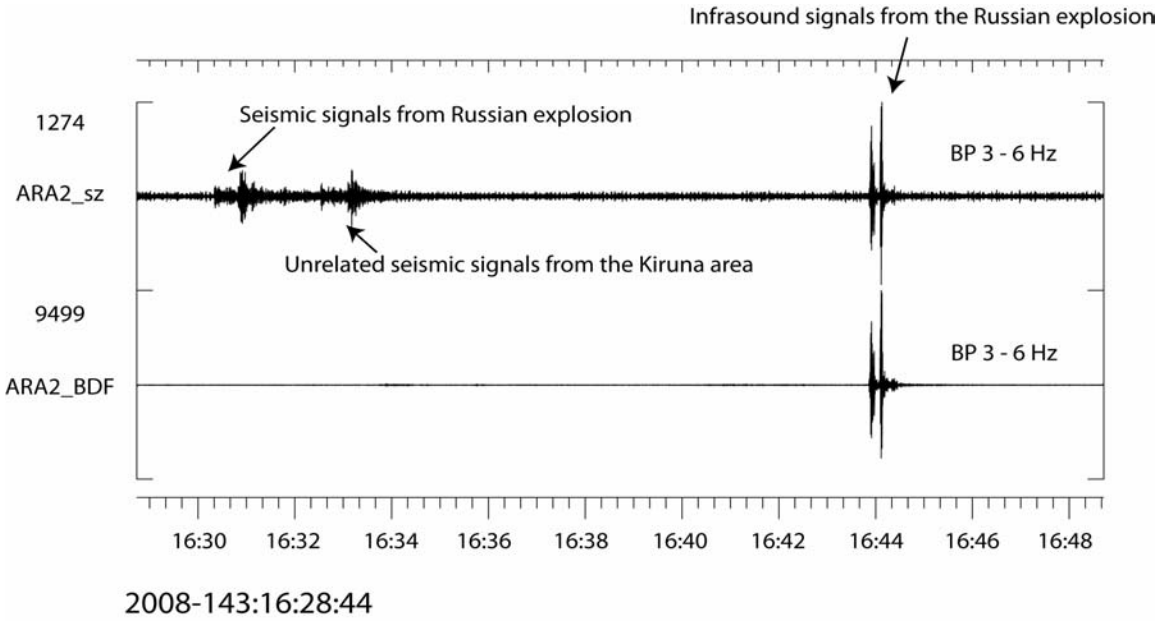

Figure 6.3.3. The figure shows two waveforms covering 20 minutes of ARCES array data and representing a presumed explosion in NW Russia on 22 May 2008. The data are filtered in a 3-6 Hz frequency band.

One interesting observation from Figure 6.3.3 is the differences in signal-to-noise ratio (SNR) between the two traces. While the SNR of the infrasonic signal is high in both cases, it is clearly superior for the microbarograph. This is by no means surprising; in fact, the most surprising feature is that the seismic trace is so close to the microbarograph trace in terms of both SNR and waveform characteristics. Also note that “noise” on the seismic trace comprises both the usual “background noise” and the actual seismic signals, which naturally are not visible on the microbarograph trace.

The similarity of the infrasonic signals on the two sensors is further illustrated in Figure 6.3.4, which shows an expanded plot in a somewhat broader frequency band (1.5-6 Hz). This similarity is even more clearly shown in Figure 6.3.5, where the two sensor traces are plotted together in the same coordinate system.

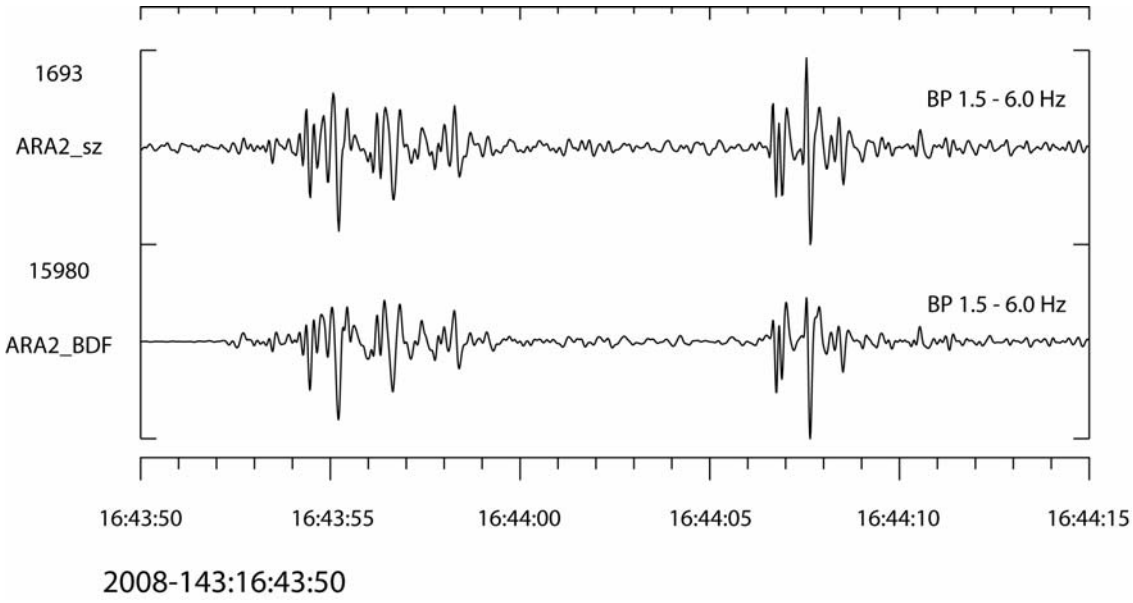

Figure 6.3.4. Expanded plot of the infrasonic signals shown in Figure 6.3.3, filtered in the1.5-6.0 Hz frequency band. Note the similarity of the signals recorded by the seismometer (top) and the microbarograph (bottom).

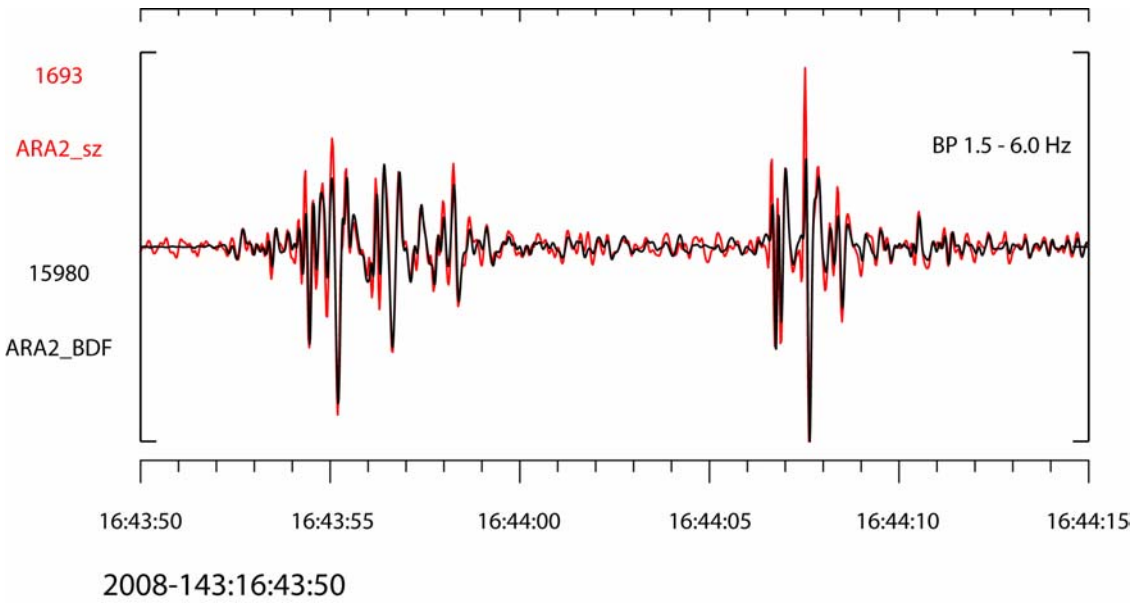

Figure 6.3.5. Same as Figure 6.3.4, but with the two sensor traces plotted in the same coordinate system.

In Figure 6.3.6, we show for comparison the infrasonic data recorded by a seismometer in the Apatity array, together with data recorded by a co-located microbarograph. Again, the similarity between the two sensors is remarkable, but in this case there is a phase delay of about 0.03 seconds between the two sensor types. This is probably due to a small difference in sensor location (of the order of 10 meters), and is in any case insignificant for our purposes.

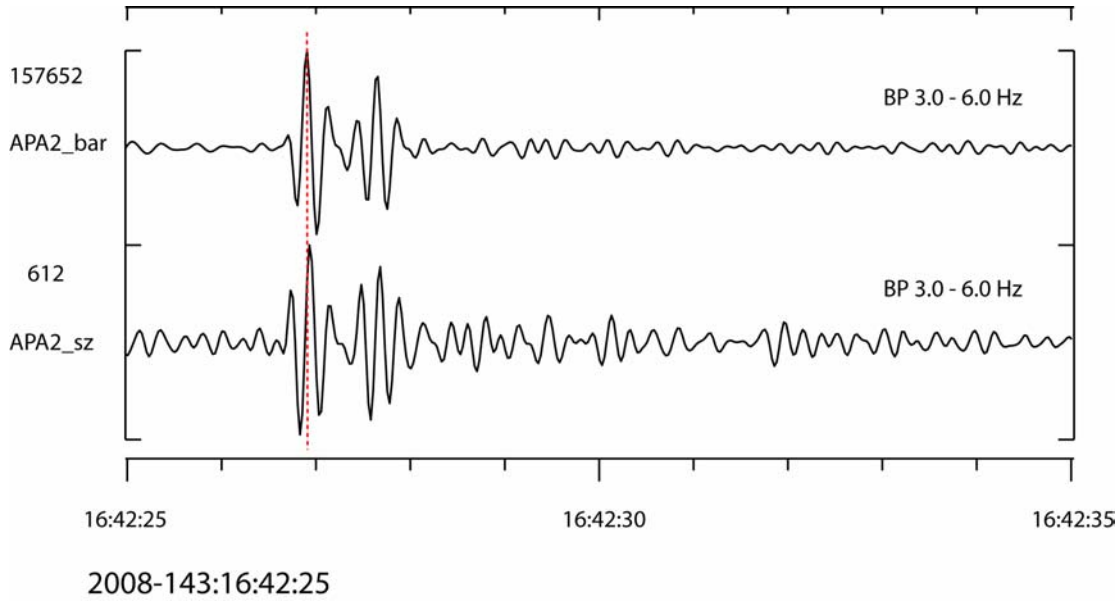

Figure 6.3.6. Recordings of the infrasonic phase at the Apatity array for the previously discussed presumed explosion in NW Russia. The traces are from a seismometer (top) and a co-located microbarograph (bottom). Note the slight phase shift between the traces.

We mention one additional feature, which is characteristic for many infrasound recordings. This feature is the presence of more than one infrasonic phase for the same event. It is well known that under various atmospheric conditions, the temporal characteristics and amplitudes of the various infrasonic phases can show great differences, even between explosions conducted in the same place and with the same source characteristics. This fact is discussed in detail by Gibbons et al. (2007) for a set of explosion from a site in northern Finland (Explosion site 1 in Figure 6.3.1).

In the example studied in the present paper, the ARCES data appears to show two infrasonic phases, separated by about 10 seconds. This might initially be interpreted as representing two separate explosions. However, by vespagram analysis of the ARCES signals (see Figure 6.3.7), it is quite clear that there is in fact only one event that causes these phase recordings.

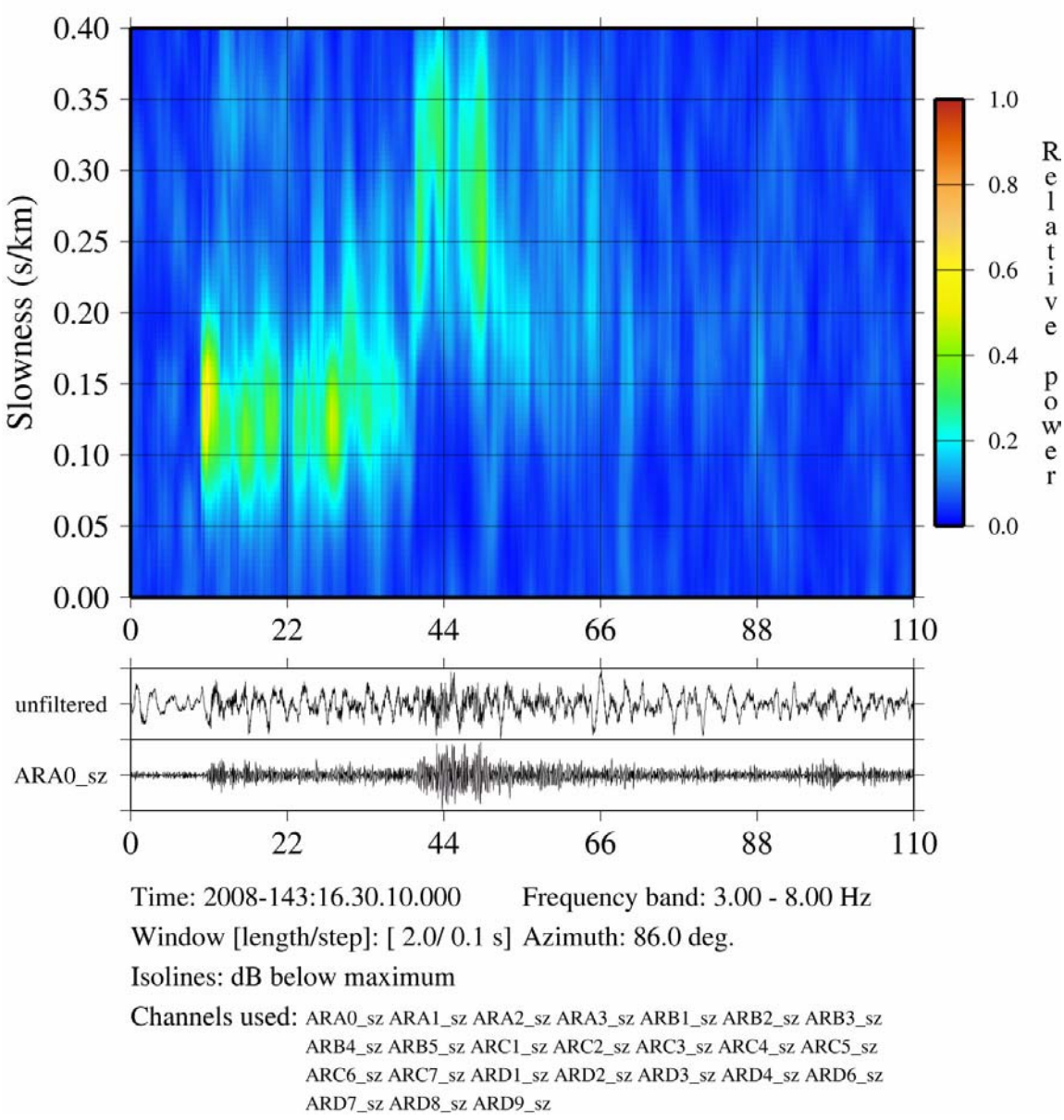

Figure 6.3.7. Vespagram of the ARCES array, steered to 86 degrees, for the time of the seismic phase recordings of the NW Russia presumed explosion. The plot indicates one P-phase and one S-phase, with no clear evidence of a second onset.

6.3.4 Slowness estimation

Figure 6.3.8 shows ARCES full seismic array slowness estimate, using 25 SPZ seismometers, for the infrasound phase of the NW Russia event discussed in this paper. The method of Frankel et al. (1991) is used for this and other slowness estimates in this paper. Figure 6.3.9 shows the slowness estimates using only the three microbarographs.

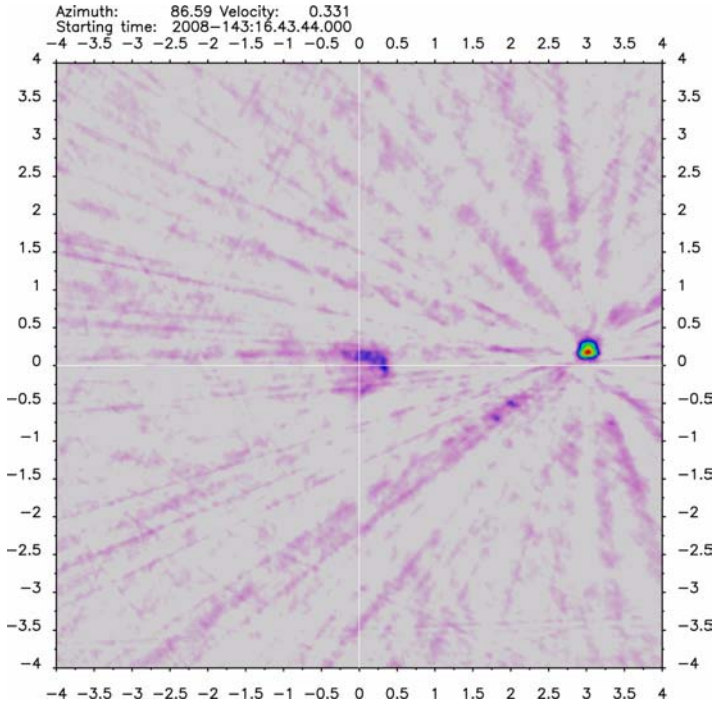

Figure 6.3.8. Slowness estimate of the infrasonic phase of the NW Russia presumed explosion, using the 25 vertical-component seismometers of the ARCES array.

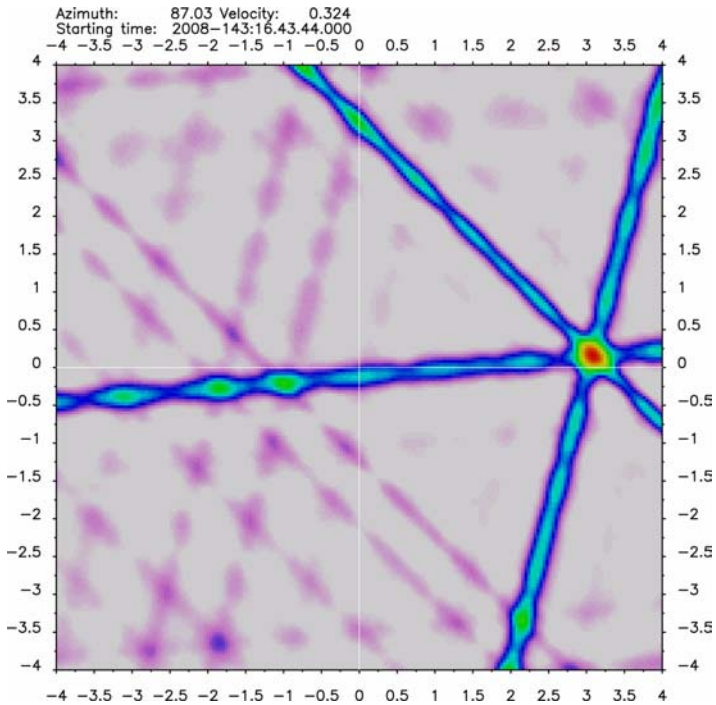

Figure 6.3.9. Slowness estimate of the NW Russia event, using only the three ARCES microbarographs.

We note that the estimated azimuth is 86.59 degrees, and the estimated velocity is 331 m/s for the full 25-element seismic array (Figure 6.3.8). For comparison, the estimated azimuth is 87.03 degrees, and the estimated velocity is 324 m/s using the three microbarographs only. Thus, the difference is very small, although the peak of the seismic plot is somewhat sharper than for the microbarograph plot. The cross-like sidelobe pattern of Figure 6.3.9 is typical of the slowness plots for a three-element array.

Figure 6.3.10 shows the slowness estimate by the Apatity microbarograph array for the infrasound phase recorded at Apatity. The sharpness of the peak is similar to that of ARCES (Figure 6.3.9), which reflects a similar array aperture (about 300 m) and a similar frequency content of the infrasonic signals. The estimated azimuth is 348.23 degrees and the estimated velocity is 340 m/s in this case. Again these are quite close to the (assumed) true values.

A noteworthy feature of Figure 6.3.10 is the color difference (green) of one of the "arms" of the cross-pattern. This occurs because one of the three microbarograph had a hardware (filter) problem at the time of the event, and therefore showed considerably poorer SNR than the other instruments. Nevertheless, the slowness estimate does not deteriorate significantly, although the effect would be more severe for lower SNR signals.

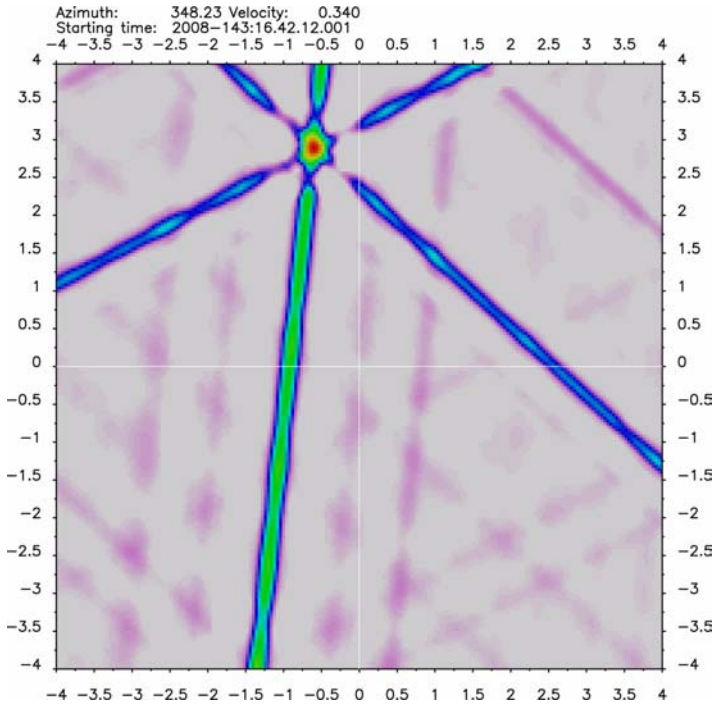

Figure 6.3.10. Slowness estimate of the NW Russia event, using the three Apatity microbarographs.

6.3.5 Swedish/Finnish network data

The Swedish/Finnish infrasound network comprises much smaller arrays than ARCES and Apatity. It could be of interest to compare the results using these arrays to what we have shown before. Figure 6.3.11a shows the waveforms recorded by the Kiruna infrasound array in northern Sweden. The SNR is in fact quite good, and the signals are not clipped (this is sometimes a problem for these arrays, which have a much more limited dynamic range than ARCES and Apatity).

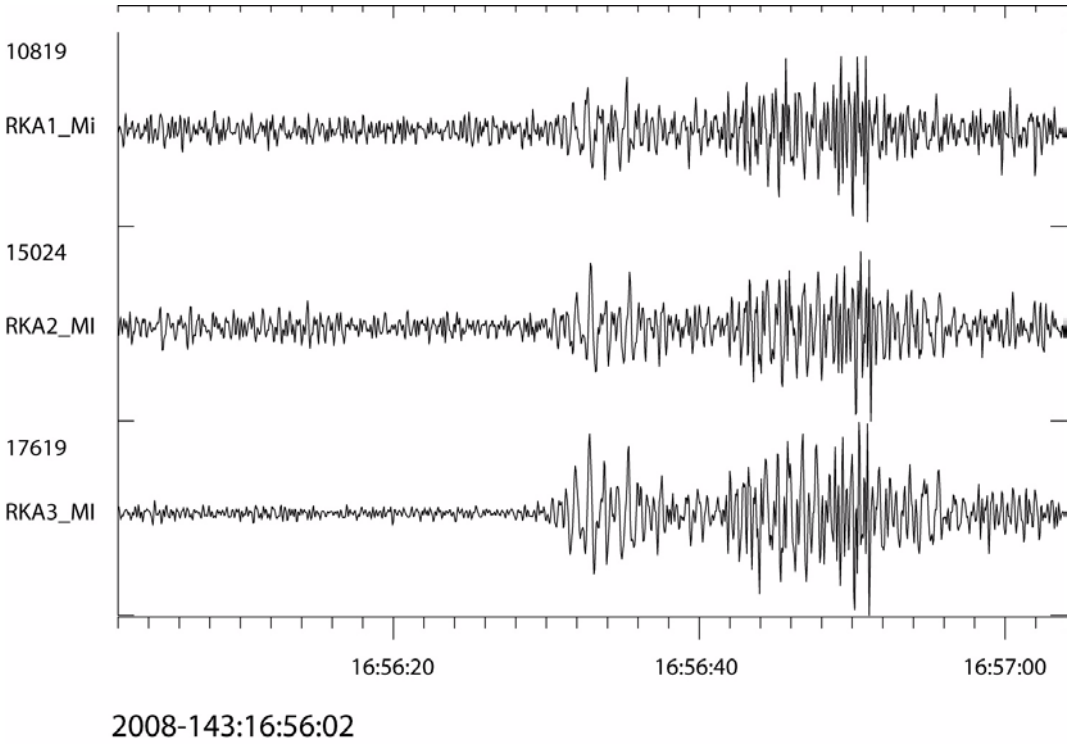

Figure 6.3.11a. Waveforms recorded by the Kiruna infrasound array in northern Sweden for the NW Russia event.

Figure 6.3.11b shows slowness estimate for the infrasound phase using data from the Kiruna infrasound array. The azimuth (81.01 degrees) is quite close to the assumed true azimuth, whereas the phase velocity (296 m/s) is somewhat lower than expected. Here, it must be remembered that the Swedish arrays have an aperture of only 75 meters, which is much less than even the small ARCES and Apatity microbarograph arrays. This causes the peak of the plot shown in Figure 6.3.11a to be much less sharp than what was seen for the ARCES and Apatity microbarograph arrays.

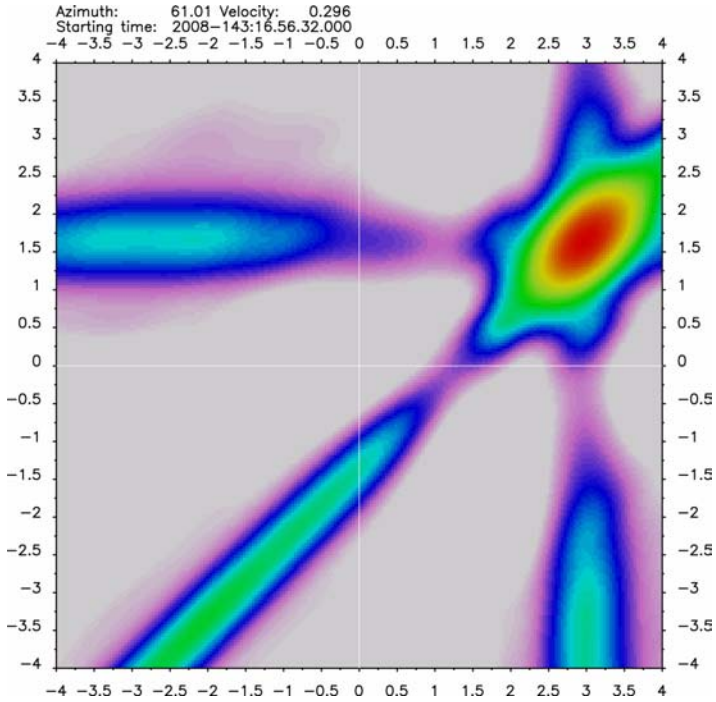

Figure 6.3.11b. Slowness estimate of the NW Russia event, using the Kiruna infrasound array.

6.3.6 Detector performance

In the 1 April - 30 June 2006 Quarterly R&D Status Report we described a slowness-based algorithm for detecting infrasound signals at the ARCES seismic array. Using the seismic sensors of A- and B-rings of the ARCES array, we ran broad-band slowness analysis (Kværna and Doornbos, 1986) with a sampling interval of 2 seconds and a window length of 10 seconds in the 2-5- Hz frequency band. We have now applied this algorithm time interval April - June 2008, and we show in Figure 6.3.12 the results for 22 May 2008. The processing algorithm can be summarized as follows:

1. Only consider slowness estimates in the velocity range 0.25-0.66 km/s (sound velocities).
2. Form groups of consecutive slowness estimates with sound velocities, with the restriction that the azimuth estimates are within 10 degrees of the first azimuth estimate of the group.
3. An infrasound detection is declared if a group has three or more elements (i.e. a duration of 6 seconds or more), and the highest slowness peak of the group is more than 0.9 dB above the 2nd peak.

We have experienced that infrasound signals almost without exceptions yields three or more consecutive slowness estimates with comparable azimuths. This restriction also prevents erroneous declarations of infrasound detections caused by spurious slowness estimates. In the cases with data quality problems (gaps, spikes) on one or more array channels, we may experience a

few ‘false’ consecutive slowness estimates with sound velocities and comparable azimuths. However, under such circumstances the maximum slowness peak is usually not well defined, so we have introduced the additional criterion requiring that the highest slowness peak of the group is more than 0.9 dB above the 2nd peak.

The red data points of Figure 6.3.12 show slowness estimates belonging to groups with three or more elements, formed as described above. The lower panel shows the number of slowness estimates chained together. Notice that for the two signals around 10:06 the numbers are 5 and 15, respectively. For the signal at 16:43, the number is 19.

Details about the 22 May 2008 infrasound detections at the ARCES seismic array are given in Table 6.3.1.

Table 6.3.1. Infrasound detections on the ARCES seismic array, 22 May 2008

Start Time	Duration	App. vel. (km/s)	Back-azi, (deg.)	Rel. Power	SNR (dB)
2008-143:10.06.06.000	8.0	0.337	166.74	0.563	4.22
2008-143:10.06.26.000	28.0	0.337	166.81	0.611	5.74
2008-143:16.43.50.000	36.0	0.329	85.56	0.749	20.93

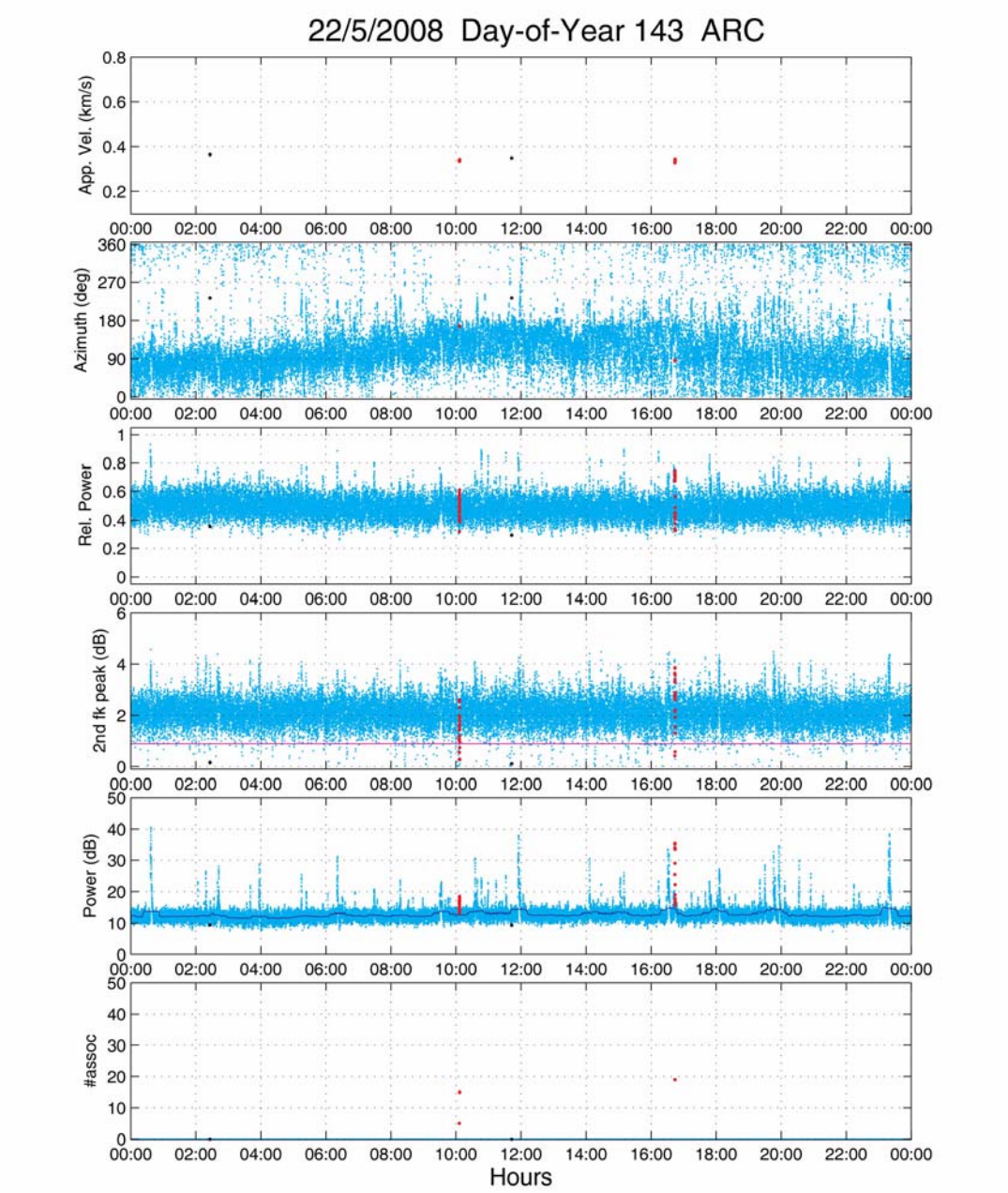

Figure 6.3.12. Processing results from continuous slowness analysis of the ARCES A- and B-ring seismic sensors for 22 May 2008. The red points represent slowness estimates from candidate infrasound signals.
1st panel: Apparent velocity. Seismic velocities fall outside the axis.
2nd panel: Back-azimuth.
3rd panel: The relative power of the slowness maximum (a coherency measure).
4th panel: The difference in decibels between the slowness maximum and the 2nd slowness peak.
5th panel: The absolute power of the slowness maximum (a signal amplitude measure). The blue line represents a smoothed average over the time interval.
6th panel: The number of slowness estimates chained together.

We have adopted a similar procedure for processing of the three ARCES microbarographs. The 22 May 2008 processing results for the ARCES microbarographs are displayed in Figure 6.3.13. Different from processing of the seismic sensors, we now almost always show get slowness estimates with sound velocities, and we had to introduce some changes to the algorithms for forming infrasound detection groups. Another issue with the microbarograph data is that we quite often have large amplitudes at only one of the sensors, probably caused by local wind or other very local noise sources. In order to identify such instances, we introduced the amplitude ratio

$$\frac{Max(a_i)}{Min(a_i)} \; i = 1,3$$

where a_i is the short-term average at sensor i. This ratio yields high values when one of the microbarographs has anomalous values. The processing algorithm applied to the microbarographs can be summarized as follows:

1. Only consider slowness estimates where $\frac{Max(a_i)}{Min(a_i)} < 3.16$ (or $log_{10} \frac{Max(a_i)}{Min(a_i)} < 0.5$)

   See 6th panel of Figure 6.3.13.

2. Only consider slowness estimates in the velocity range 0.25-0.66 km/s (sound velocities). See 1st panel of Figure 6.3.13.

3. Calculate the relative power median and the inter-quartile range (iqr) for the entire time interval. Only consider slowness estimates with relative power values exceeding the median + 1.5 *iqr. This threshold is shown by the red line in the 3rd panel of Figure 6.3.13.

4. Form groups of consecutive slowness estimates with sound velocities, with the restriction that the azimuth estimates are within 10 degrees of the first azimuth estimate of the group.

5. An initial infrasound detection is declared if a group has four or more elements. See 7th panel of Figure 6.3.13.

6. Calculate the amplitude SNR of the individual slowness estimates using the long-term average of the absolute slowness power as the reference (see 5th panel of Figure 6.3.13). For definition of infrasound detection groups having a short duration, we required an SNR of about 4 dB, shown by the red line in the 5th panel of Figure 6.3.13.

Details about the 22 May 2008 infrasound detections at the ARCES microbarographs are given in Table 6.3.2, and we see a much higher number of detections than for the ARCES seismic sensors. The microbarograph infrasound detections corresponding to those found on the seismic sensors (see Table 6.3.1) are marked red. For readability the infrasound detection falling within one-hour intervals are highlighted.

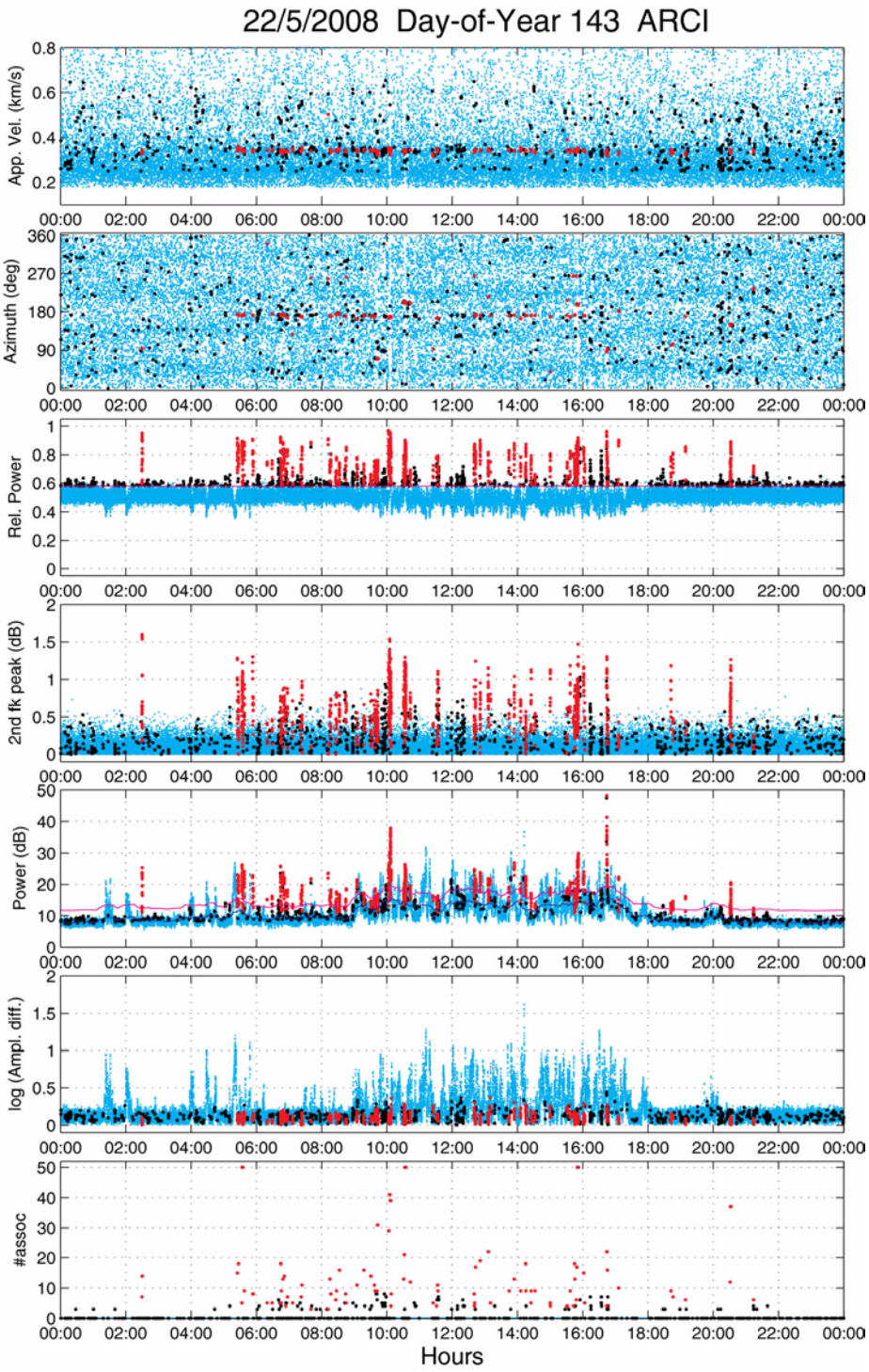

Figure 6.3.13. Processing results from continuous slowness analysis of the three ARCES microbarograph sensors for 22 May 2008. The red points represent slowness estimates from candidate infrasound signals.
1st panel: Apparent velocity.
2nd panel: Back-azimuth.
3rd panel: The relative power of the slowness maximum (a coherency measure).

4th panel: The difference in decibels between the slowness maximum and the 2nd slowness peak.
5th panel: The absolute power of the slowness maximum (a signal amplitude measure). The blue line represents a smoothed average over the time interval.
6th panel: Maximum amplitude difference among the three microbarograph sensors.
7th panel: The number of slowness estimates chained together.

Table 6.3.2. Infrasound detections on the ARCES microbarographs, 22 May 2008

Start Time	Duration	App. vel. (km/s)	Back-azi, (deg.)	Rel. Power	SNR (dB)
2008-143:02.29.26.000	12.0	0.332	93.51	0.729	4.44
2008-143:02.29.50.000	26.0	0.326	93.69	0.950	16.79
2008-143:05.24.54.000	28.0	0.342	172.11	0.913	11.47
2008-143:05.26.48.000	34.0	0.339	171.02	0.864	11.09
2008-143:05.33.24.000	8.0	0.344	170.16	0.857	6.78
2008-143:05.33.36.000	104.0	0.340	171.05	0.892	14.58
2008-143:05.37.44.000	16.0	0.340	172.91	0.884	13.48
2008-143:05.53.04.000	14.0	0.343	171.32	0.907	13.49
2008-143:05.54.04.000	14.0	0.344	171.28	0.822	9.78
2008-143:06.19.42.000	8.0	0.343	340.46	0.749	6.51
2008-143:06.29.00.000	8.0	0.342	174.24	0.759	7.69
2008-143:06.44.26.000	8.0	0.335	174.07	0.922	16.19
2008-143:06.44.38.000	34.0	0.332	173.72	0.898	13.18
2008-143:06.45.40.000	8.0	0.339	170.09	0.714	4.35
2008-143:06.45.54.000	16.0	0.340	170.39	0.645	3.87
2008-143:06.48.32.000	24.0	0.336	173.37	0.883	14.15
2008-143:06.51.12.000	26.0	0.336	172.72	0.837	12.41
2008-143:06.54.04.000	6.0	0.337	168.58	0.701	4.62
2008-143:06.56.58.000	12.0	0.337	165.26	0.833	8.84
2008-143:07.06.30.000	8.0	0.347	127.73	0.707	5.00
2008-143:07.22.08.000	12.0	0.336	168.25	0.770	8.01
2008-143:07.23.46.000	20.0	0.346	167.22	0.852	10.60
2008-143:07.40.20.000	4.0	0.339	259.74	0.885	12.22
2008-143:08.11.54.000	4.0	0.504	256.97	0.910	14.02
2008-143:08.15.02.000	24.0	0.342	171.19	0.755	7.02
2008-143:08.16.42.000	14.0	0.336	168.01	0.804	8.93
2008-143:08.25.54.000	10.0	0.339	173.35	0.676	5.07
2008-143:08.27.08.000	16.0	0.335	172.25	0.781	8.22
2008-143:08.32.30.000	30.0	0.347	174.22	0.743	7.58
2008-143:08.44.10.000	14.0	0.341	169.06	0.772	6.41
2008-143:08.45.14.000	8.0	0.333	261.08	0.851	9.70
2008-143:09.04.50.000	20.0	0.337	163.02	0.780	8.94

Table 6.3.2. Infrasound detections on the ARCES microbarographs, 22 May 2008

Start Time	Duration	App. vel. (km/s)	Back-azi, (deg.)	Rel. Power	SNR (dB)
2008-143:09.17.24.000	30.0	0.337	168.42	0.736	4.26
2008-143:09.30.18.000	26.0	0.339	169.49	0.662	3.04
2008-143:09.36.50.000	20.0	0.340	168.23	0.753	3.66
2008-143:09.38.18.000	16.0	0.339	168.03	0.760	6.67
2008-143:09.41.38.000	16.0	0.331	69.89	0.712	2.87
2008-143:09.42.24.000	60.0	0.341	68.48	0.762	4.37
2008-143:10.02.58.000	56.0	0.340	167.68	0.969	11.49
2008-143:10.04.30.000	80.0	0.337	166.91	0.907	15.81
2008-143:10.05.54.000	76.0	0.334	166.81	0.955	22.89
2008-143:10.07.18.000	6.0	0.336	165.88	0.706	6.74
2008-143:10.07.46.000	14.0	0.348	166.94	0.814	9.19
2008-143:10.30.38.000	24.0	0.343	201.56	0.795	4.45
2008-143:10.31.50.000	40.0	0.338	201.78	0.799	6.23
2008-143:10.33.04.000	132.0	0.338	201.67	0.900	11.90
2008-143:10.42.56.000	22.0	0.341	201.06	0.692	6.55
2008-143:11.25.00.000	8.0	0.327	92.44	0.725	4.14
2008-143:11.31.14.000	6.0	0.347	164.24	0.783	4.09
2008-143:11.33.04.000	20.0	0.340	164.59	0.722	2.46
2008-143:11.33.38.000	16.0	0.338	164.50	0.793	4.69
2008-143:12.40.24.000	14.0	0.340	171.68	0.855	6.79
2008-143:12.40.48.000	6.0	0.333	264.44	0.829	10.50
2008-143:12.41.18.000	8.0	0.336	264.78	0.872	8.70
2008-143:12.42.34.000	32.0	0.341	170.86	0.822	7.51
2008-143:12.51.16.000	36.0	0.337	170.73	0.901	10.24
2008-143:13.06.06.000	42.0	0.342	215.08	0.814	7.81
2008-143:13.10.10.000	8.0	0.339	171.13	0.752	7.62
2008-143:13.44.22.000	16.0	0.342	170.50	0.827	5.82
2008-143:13.53.54.000	24.0	0.338	172.46	0.877	13.02
2008-143:14.05.48.000	16.0	0.338	163.02	0.786	7.07
2008-143:14.14.50.000	34.0	0.341	170.67	0.850	10.71
2008-143:14.15.28.000	16.0	0.340	171.10	0.870	10.29
2008-143:14.24.50.000	8.0	0.339	171.20	0.744	5.58
2008-143:14.25.06.000	16.0	0.344	170.76	0.794	4.69
2008-143:14.32.16.000	16.0	0.333	170.78	0.661	2.26
2008-143:15.00.08.000	8.0	0.338	167.63	0.711	4.90
2008-143:15.00.18.000	6.0	0.340	39.81	0.804	5.54
2008-143:15.30.44.000	6.0	0.339	171.12	0.648	4.30
2008-143:15.31.26.000	6.0	0.389	206.73	0.748	5.13
2008-143:15.36.54.000	16.0	0.338	168.00	0.822	6.57

Table 6.3.2. Infrasound detections on the ARCES microbarographs, 22 May 2008

Start Time	Duration	App. vel. (km/s)	Back-azi, (deg.)	Rel. Power	SNR (dB)
2008-143:15.42.40.000	6.0	0.338	263.95	0.804	7.17
2008-143:15.44.44.000	34.0	0.342	171.42	0.800	4.81
2008-143:15.45.24.000	24.0	0.343	172.07	0.713	-1.15
2008-143:15.48.08.000	10.0	0.335	263.99	0.862	7.36
2008-143:15.49.00.000	32.0	0.344	198.98	0.740	1.98
2008-143:15.50.00.000	126.0	0.340	197.09	0.917	15.68
2008-143:16.01.42.000	28.0	0.343	170.49	0.848	9.72
2008-143:16.03.44.000	8.0	0.334	169.70	0.732	4.04
2008-143:16.43.52.000	6.0	0.325	86.27	0.961	39.90
2008-143:16.44.02.000	42.0	0.342	85.88	0.935	38.25
2008-143:16.45.00.000	30.0	0.319	92.12	0.781	7.51
2008-143:17.05.50.000	18.0	0.333	182.80	0.900	8.56
2008-143:18.42.02.000	16.0	0.326	101.30	0.784	5.92
2008-143:18.45.54.000	12.0	0.329	104.94	0.809	6.52
2008-143:19.09.00.000	10.0	0.333	168.36	0.853	8.33
2008-143:20.30.56.000	22.0	0.340	149.19	0.753	5.15
2008-143:20.31.32.000	72.0	0.334	148.81	0.889	12.40
2008-143:21.14.10.000	10.0	0.334	234.27	0.721	4.54

Figure 6.3.14 shows more details about the infrasound detections at the ARCES seismic sensor for the time interval 10:00 - 11:00 on 22 May 2008. The two detections at 10:06 have very similar back-azimuths (166 degrees) and apparent velocities (0.337 km/s), and are most likely attributed to the same signal.

The detections at the three ARCES microbarographs for the 10:00 - 11:00 time interval are shown in Figure 6.3.15. The five infrasound detections within the time interval 10:03 - 10:08 have all similar back-azimuths (165-167 degrees) and apparent velocities (0.334-0.348 km/s). The corresponding waveforms are shown in Figure 6.3.16, where the time intervals of the infrasound detections are highlighted red. The waveforms plot clearly show that the declared detections correspond to separate infrasound signal pulses. The group of three infrasound detections between 10:30 and 10:35 show the same type of characteristics with separate signal pulses having similar back azimuths (201 degrees) and apparent velocities (0.338 - 0.343 km/s).

The microbarograph waveform plot of Figure 6.3.16 show several instances where one of the sensors has anomalous amplitudes. However, the previously described method for identifying such instances efficiently prevent any infrasound detections within such time intervals.

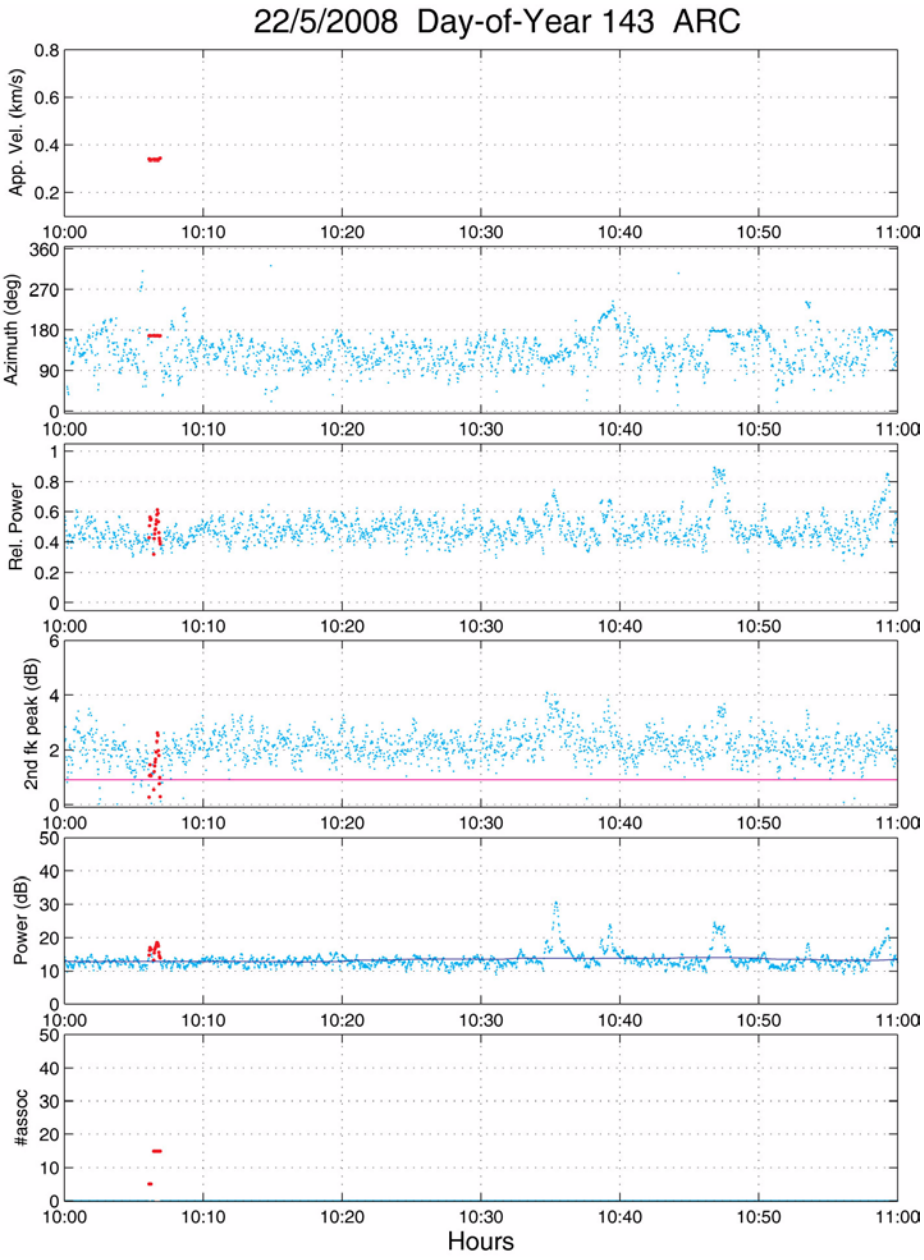

Figure 6.3.14. Processing results from continuous slowness analysis of the ARCES A- and B-ring seismic sensors for 10:00 - 11:00 GMT on 22 May 2008. The red points represent slowness estimates from candidate infrasound signals. See caption of Figure 6.3.12 for details.

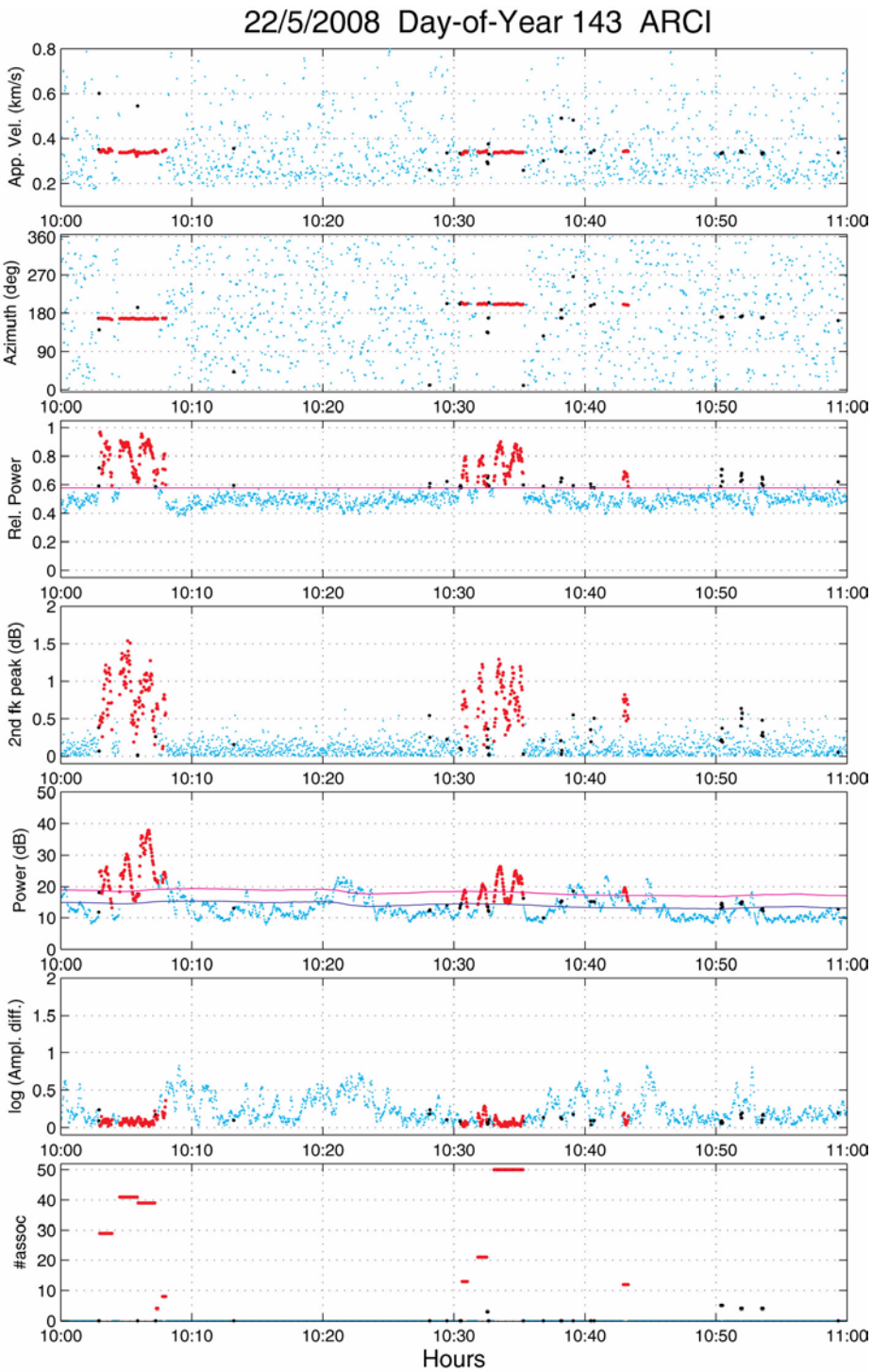

Figure 6.3.15. Processing results from continuous slowness analysis of the three ARCES microbarograph sensors for 10:00 -11:00 on 22 May 2008. The red points represent slowness estimates from candidate infrasound signals. See caption of Figure 6.3.13 for details.

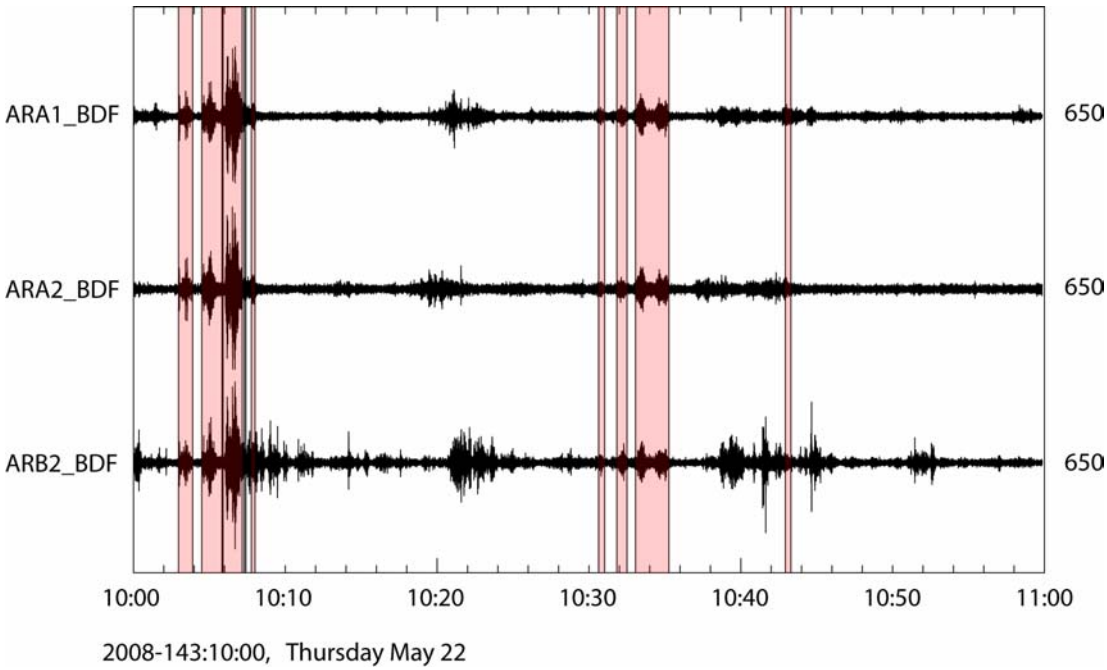

Figure 6.3.16. ARCES microbarograph data for the time interval 10:00 -11:00 on 22 May 2008, bandpass filtered between 2.0 and 5.0 Hz. Time intervals with infrasound signal detections (see Table 6.3.2) are shown red.

Figure 6.3.17 shows the infrasound processing results for the ARCES seismic sensors for the time interval 16:00 - 17:00 on 22 May 2008. During this time interval there is only one detection at 16:43:50, corresponding to the infrasound signals from the Russian explosion site previously described in this paper. The corresponding processing results and waveform plot for the three ARCES microbarographs are shown in Figures 18 and 19.

As a final example, we show in Figures 20 and 21 infrasound processing results and waveform plot at the ARCES microbarographs for the time interval 05:00 - 06:00 on 22 May 2008. Seven infrasound detections are found during this time interval, having durations ranging from 8 to 104 seconds. All detections show similar back-azimuths (170 - 173 degrees) and typical sound velocities (0.34 km/s), indicating a common source for these signals. No infrasound detections at the seismic sensors are found during this time interval.

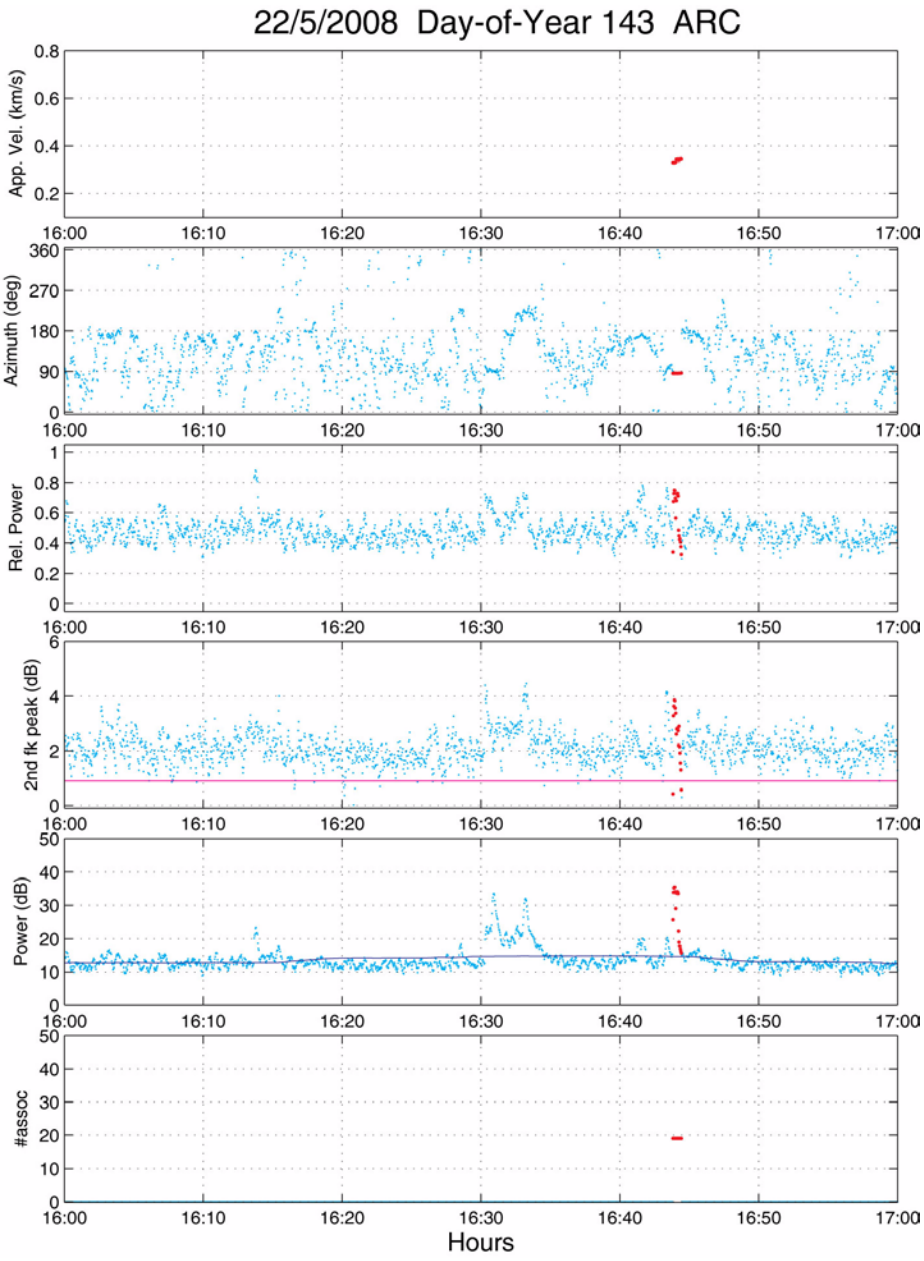

Figure 6.3.17. Processing results from continuous slowness analysis of the ARCES A- and B-ring seismic sensors for 16:00 - 17:00 GMT on 22 May 2008. The red points represent slowness estimates from candidate infrasound signals. See caption of Figure 6.3.12 for details.

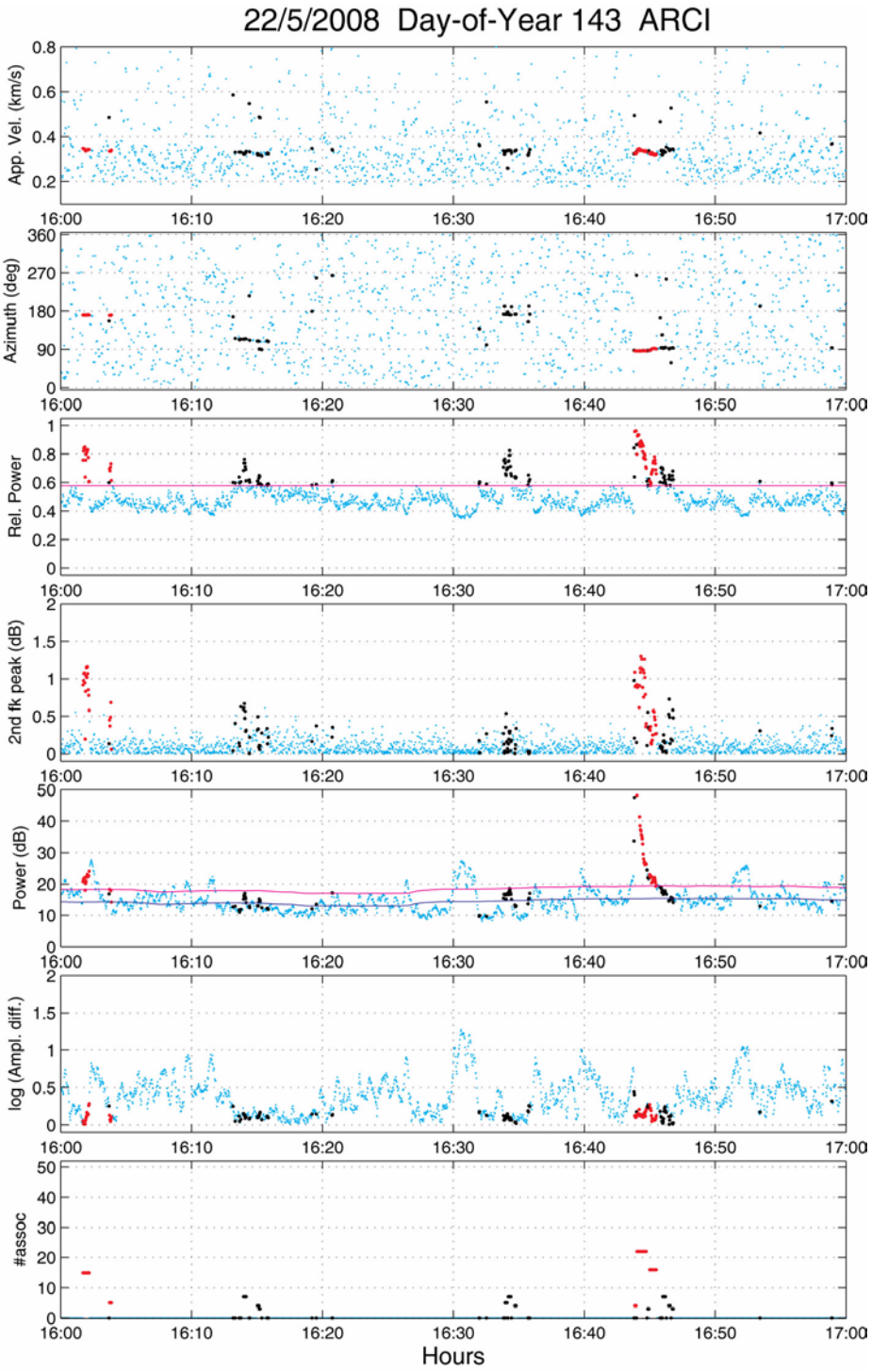

Figure 6.3.18. Processing results from continuous slowness analysis of the three ARCES microbarograph sensors for 16:00 -17:00 on 22 May 2008. The red points represent slowness estimates from candidate infrasound signals. See caption of Figure 6.3.13 for details.

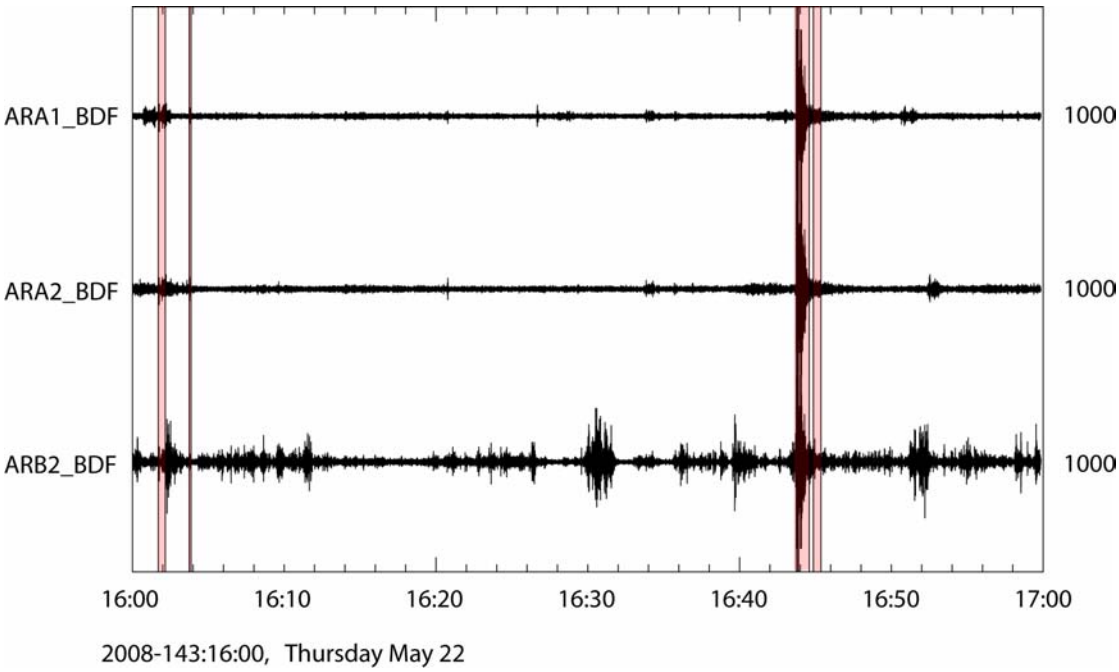

Figure 6.3.19. ARCES microbarograph data for the time interval 16:00 -17:00 on 22 May 2008, bandpass filtered between 2.0 and 5.0 Hz. Time intervals with infrasound signal detections (see Table 6.3.2) are shown red.

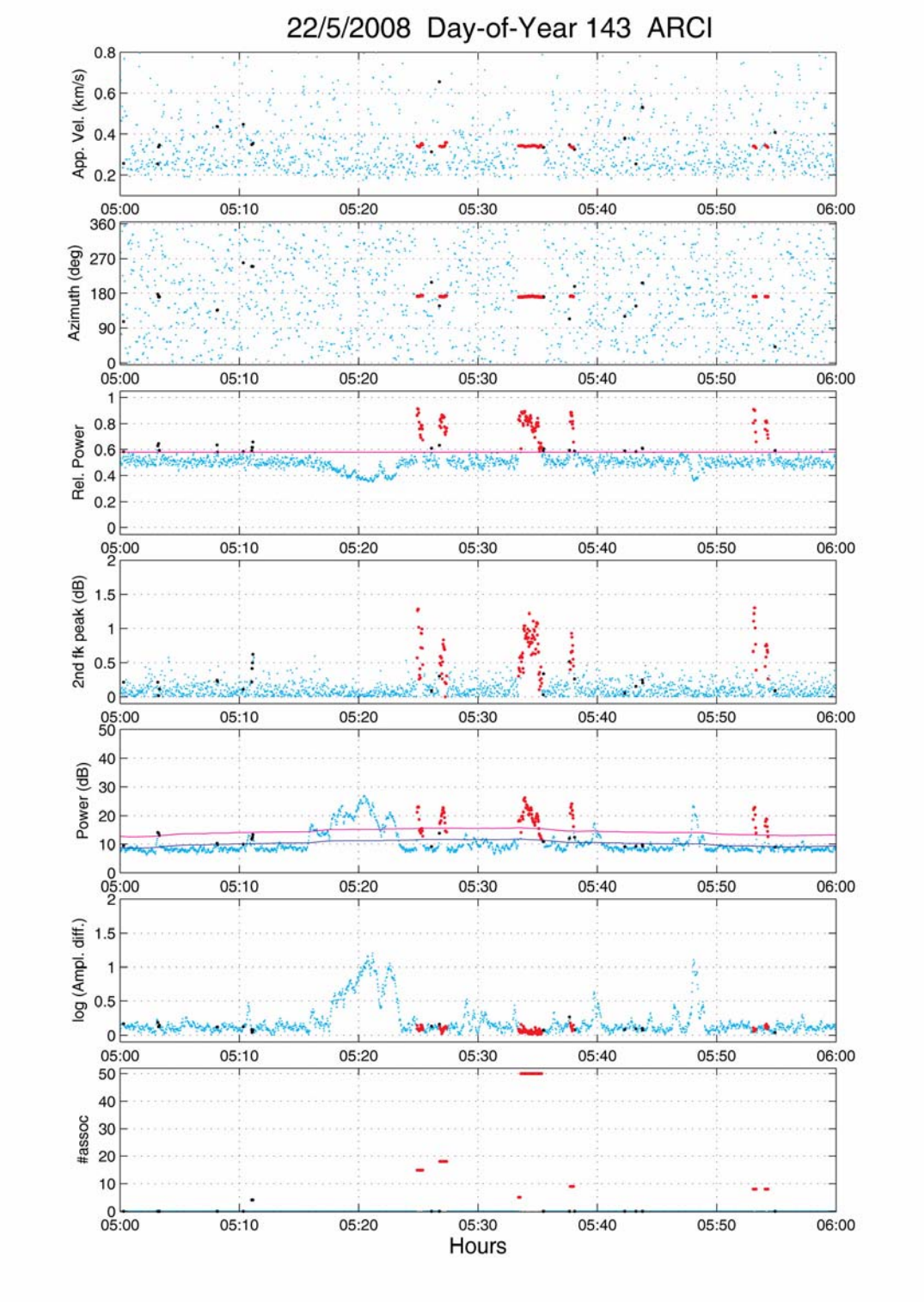

Figure 6.3.20. Processing results from continuous slowness analysis of the three ARCES microbarograph sensors for 05:00 -06:00 on 22 May 2008. The red points represent slowness estimates from candidate infrasound signals. See caption of Figure 6.3.13 for details.

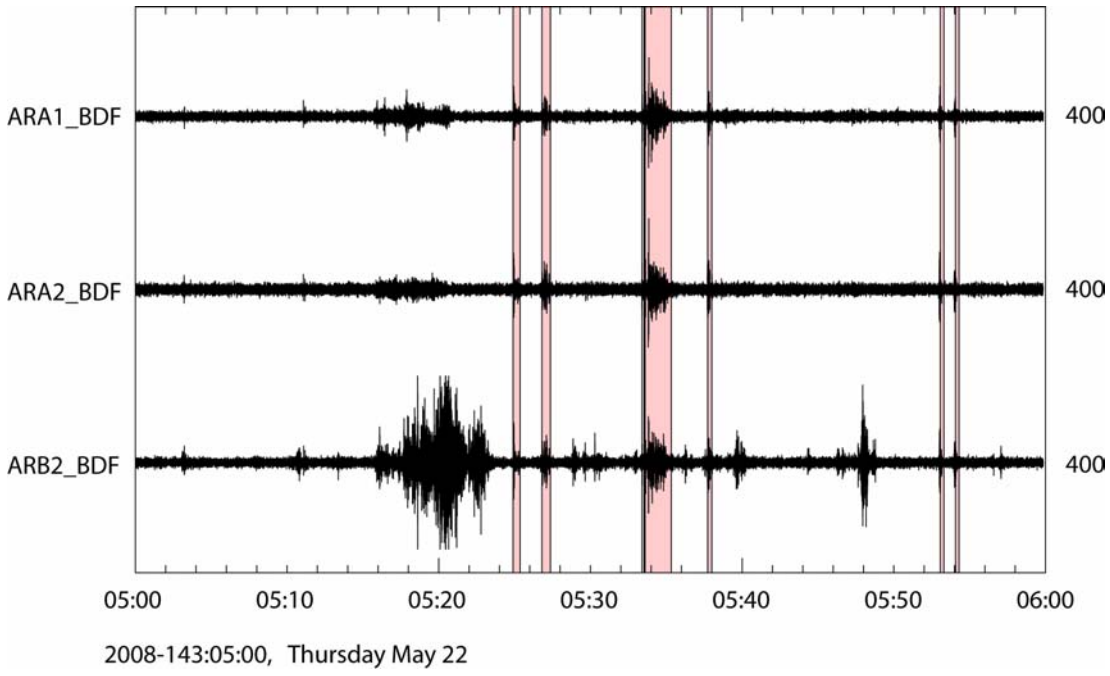

Figure 6.3.21. ARCES microbarograph data for the time interval 05:00 -06:00 on 22 May 2008, bandpass filtered between 2.0 and 5.0 Hz. Time intervals with infrasound signal detections (see Table 6.3.2) are shown red.

We have demonstrated that an infrasound signal detector based on continuous slowness analysis is applicable both to the seismometer and microbarograph data at the ARCES array. To avoid spurious detections at the microbarographs, additional constraints had to put on the SNR of the signals. Data quality checks were introduced to discard instances where sensors show anomalous amplitudes. A much larger number of detections are found on the microbarograph data, clearly illustrating the improved sensitivity to infrasound signals as compared to recordings at the seismic sensors.

In parallel with this study, we have processed the same data set using cross-correlation techniques (Gibbons et al., 2007) combined with the detection statistic of Brown et al. (2002). These results are comparable to those presented in this study, but a detailed comparison will require further work concerning setting of window and filter parameters, threshold setting and data quality control.

For the time interval April - June 2008 we have also processed the infrasound data from Apatity, as well as from the stations of the Swedish Infrasound Network using the method described above. A natural next step is to combine the signal detections from this dense network of six infrasound stations in Northern Europe to obtain information about the infrasound sources.

6.3.7 References

Baryshnikov (2004). Research of infrasound background characteristics for estimation of threshold sensitivity of infrasound method for test monitoring. Final Technical Report ISTC 1341-01 (part 1 of total 2), International Science and Technology Center (ISTC), Moscow, 255pp.

Brown, D. J., C. N. Katz, R. Le Bras, M. P. Flanagan, J. Wang and A. K. Gault (2002). Infrasonic signal detection and source location at the prototype international data centre, *Pure Appl. Geophys*, **159**, 1081-1125.

Frankel, A., S. Hough, P. Friberg and R. Busby (1991): Observations of Loma Prieta aftershocks from a dense array in Sunnyvale, California, Bull. Seism. Soc. Am. 81, 1900-1922

Gibbons, S. G., F. Ringdal and T. Kværna (2007). Joint seismic-infrasonic processing of recordings from a repeating source of atmospheric explosions, *J. Acoust. Soc. Am.*, **122**, EL158-EL164.

Kværna, T. and D. J. Doornbos (1986). An integrated approach to slowness analysis with arrays and three-component stations, *Semiann. Tech. Summary,* 1October 1985 - 31 March 1986, NORSAR Sci. Rep. No. 2-85/86, Kjeller, Norway.

Liszka, L. (2007): Infrasound - A summary of 35 years of infrasound research, Manuscript submitted for printing, 150 pp

Ringdal, F., and J. Schweitzer (2005). Seismic/Infrasonic Processing: Case study of explosions in NW Russia, Semiannual Technical Summary, NORSAR Scientific Report No. 2 - 2005. NORSAR, Kjeller, Norway. pp. 54-68.

Frode Ringdal
Tormod Kværna
Steven Gibbons